DRAFT VERSION SEPTEMBER 22, 2020
Typeset using LaTeX **twocolumn** style in AASTeX62

Detecting Carbon Chains In High-Mass Starless Clumps

KADIN WORTHEN,[1,2] BRIAN E. SVOBODA,[1] JUERGEN OTT,[1] AND DAVID MEIER[3,1]

[1]*National Radio Astronomy Observatory, 1003 Lopezville Rd, Socorro, NM 87801 USA*
[2]*School of Earth and Space Exploration, Arizona State University, Tempe, AZ 85281 USA*
[3]*New Mexico Institute of Mining and Technology, 801 Leroy Pl., Socorro, NW 87801 USA*

ABSTRACT

We present observations of the carbon chain molecules HC_5N, CCS, and HC_7N in the 22-25 GHz band towards 12 high-mass 70 μm dark clumps (SMDC), that have been previously found to have low-mass protostellar activity, with the Jansky Very Large Array (VLA). We detect HC_5N and CCS towards 11 out of 12 of these SMDC sources. We do not find any clear HC_7N detections in the 12 sources initially, but by averaging all the HC_7N spectra together, we do detect HC_7N in these sources. We calculate column densities and the abundances relative to H_2 for HC_5N and CCS. The average column density for HC_5N is $(2.78\pm0.46)\times10^{12}$ cm^{-2} and for CCS is $(3.66\pm0.49)\times10^{12}$ cm^{-2}. The average abundance relative to H_2 for HC_5N is found to be $(1.04\pm.3)\times10^{-9}$ and for CCS it is found to be $(1.10\pm.3)\times10^{-9}$. We compare our measured abundances of HC_5N to dark cloud chemistry models which show the abundance of HC_5N as the clumps evolve over time. In comparing our measured HC_5N abundances with dark cloud chemistry models, we determine that the 11 clumps with carbon chain detections are most likely less than approximately 1 Myr old. This result favors that these clumps are not evolved enough to have formed high-mass stars and will potentially go on to form high-mass stars at later times. This is also consistent with the idea that low-mass stars form early within clumps ($<$ 1 Myr) and high-mass stars take longer to form.

Keywords: stars: formation — ISM: clouds — ISM: molecules — ISM: structure

1. INTRODUCTION

High-mass stars ($>8M_\odot$) are influential in the evolution of galaxies and the interstellar medium (ISM), but the initial stages and conditions of high-mass star formation (HMSF) are still poorly understood (Beuther et al. 2007; Motte et al. 2018). Likewise, the formation processes involved in forming high-mass stars are far less understood compared to low-mass star formation (Motte et al. 2018). Further observations on the initial physical and chemical conditions of protocluster formation are necessary for a better understanding of HMSF. Observations of the inceptive evolutionary stages of high-mass star formation are not easily obtained since high-mass stars evolve more quickly and are less common than low-mass stars. High-mass stars are thought to form in cold and dense molecular clouds and appear to mainly form in clusters and are therefore quite obscured by the dense gas of the molecular clouds in which they form (Lada & Lada 2003; Battersby et al. 2010). Thus, our understanding of the initiation of HMSF and protocluster evolution is dependent on observing and identifying the physical and chemical properties of starless molecular cloud clumps.

Corresponding author: Kadin Worthen
kdworthe@asu.edu

The distinction between clumps and molecular clouds is that molecular clouds are composed of sub-units called clumps which are coherent regions that can have their own substructure (Bergin & Tafalla 2007). Clumps have masses in a range of 50-500 $M_\odot$ and cores have masses in a range of 10^3-10^4 $M_\odot$, but clumps are 10 to 100 times denser than clouds (Bergin & Tafalla 2007). The distinction between clumps and cores is that clumps evolve into protoclusters while cores produce individual or small groups of stars. Clumps tend to be 10-100 times as massive as individual cores and cores are on the order of 0.03-.2 pc while clumps are on the order of 0.3-3 pc (Bergin & Tafalla 2007). The disticnction between clumps, clouds, and cores is important to note because it is in molecular clumps that protoclusters and high-mass stars are thought to form (Battersby et al. 2010).

While the processes involved in the formation of high-mass stars in molecular clumps are poorly understood, a current theory of high-mass star formation involves the accretion of gas onto cores through gravitationally driven inflows (Smith et al. 2009). This process involves the clump going through gravitational collapse, caused by the gravitational potential of the gas, which channels mass towards the center of the clump. Here the gas will be accreted by the progenitors of high-mass stars that have the biggest accretion radii (Smith et al. 2009). Since molecular clumps are thought to be the region of formation of high-mass stars, observations of the physical and

chemical properties of high-mass molecular clumps provide constraints on the initial physical conditions of high-mass star and cluster formation.

Recent surveys of dust continuum emission at millimeter and far-infrared (FIR) wavelengths have discovered large samples of molecular cloud clumps, which allows for the study of the initial conditions and early stages of HMSF and protocluster evolution. One such survey is the Bolocam Galactic Plane Survey (Rosolowsky et al. 2010; Aguirre et al. 2011; Ginsburg et al. 2013; Svoboda et al. 2016), which identified over 8000 molecular cloud clumps (Svoboda et al. 2016). Sources identified via Galactic Plane surveys can be identified as Starless Clump Candidates (SCCs) by checking for star formation indicators, including 70 μm compact sources, H_2O and CH_3OH masers, and ultra compact H_{II} regions (Svoboda et al. 2016). By investigating the physical properties of these starless clump candidates, the early stages of HMSF can be better understood. One key aspect of HMSF that remains to be understood are the timescales that are involved in the formation of initial high-mass stars.

One method to investigate this question of the timescale of HMSF, is to probe the chemistry of molecular cloud clumps. Knowledge of the chemical composition of molecular clouds is a powerful diagnostic that can be used to determine the physical conditions and evolutionary stages of HMSF, and with the development of high angular resolution interferometers, we can probe the chemistry of individual cores of high-mass star forming regions (HMSFRs) (Taniguchi et al. 2019).

More specifically, carbon chain molecules are thought to be good tracers of the evolution of star forming regions (Hirota et al. 2009). They are formed by gas phase reactions involving carbon atoms and carbon cations (C^+) in young molecular clouds before carbon atoms become locked up in CO molecules (Taniguchi et al. 2018). Carbon chain molecules have been observed around low-mass protostars and are thought to form in these regions via a process called Warm Carbon Chain Chemistry (WCCC) (Sakai & Yamamoto 2013). WCCC involves carbon chains forming in warm gas from reactions involving CH_4, which sublimates off of dust grains, which is the initial process involved in WCCC.

The formation of carbon chain species happens at early times within the clump before the carbon atoms are locked up in CO molecules and they then decrease in abundances at later stages in the lifetime of the clumps due to reactions with hydrogen and helium ions and oxygen atoms, as well as depletion onto dust grains and photo-dissociation by UV photons (Sakai & Yamamoto 2013). Thus, carbon chains are thought to be an early time species in molecular cloud clumps as they are abundant in starless cores and depleted in further evolved star forming molecular clumps (Taniguchi et al. 2018). Hence, carbon chain molecules can be used to probe the evolutionary stage of molecular cloud clumps. To that end, we investigate the carbon chain chemistry of 12 starless clump candidates identified via the Bolocam Galactic Plane Survey to probe their evolutionary stages using the Jansky Very Large Array (VLA).

In this paper we present observations of carbon chain molecules towards 12 starless clump candidates that were identified from the Bolocam Galactic Plane Survey (Svoboda et al. 2016). We provide a description of the observations and target properties in Section 2. We describe our methods in obtaining the spectra in Section 3. We report column densities and abundances as well as compare our results to dark cloud chemistry models in Section 4. We discuss the implications of these results in relation to HMSF in Section 5 and conclude in Section 6.

2. OBSERVATIONS

2.1. *Molecular Line Observations*

As part of a VLA NH_3 survey of high-mass Starless Clump Candidates (SCCs; Svoboda et al. *in prep*), we simultaneously observed a suite of carbon chain molecules using the WIDAR correlator. The observations were made in D configuration with a synthesized beam of $\theta_{\rm syn} \approx 3\farcs4$ and a field of view of around 2.6 arcminutes or 3.5 pc. To see a description of how the data were calibrated see Svoboda et al. *in prep*.

These 12 clumps were identified through the combination of the images and catalogs from 2 dust continuum Galactic Plane surveys: (1) the Bolocam Galactic Plane Survey at 1.1 mm and (2) the Peretto & Fuller (2009) infrared dark cloud (IRDC) catalog. These sources were identified to be dark at 70 μm by visual inspection in Svoboda et al. (2016) and these 12 specific targets are chosen because they are the highest mass SCCs within a distance of 5 pc.

We observe the HC_5N $J = 9 \rightarrow 8$, CCS $J_N = 2_1 \rightarrow 1_0$, HC_7N $J = 20 \rightarrow 19$, and HC_7N $J = 21 \rightarrow 20$ transitions with the VLA towards these 12 clumps. The spectra for HC_5N, CCS and the $J = 20 \rightarrow 19$ transition of HC_7N all have 100 channels and the number of channels for the $J = 21 \rightarrow 20$ transition of HC_7N is 126. The rest frequencies and channel width of each of the carbon chain transitions we observed are shown in Table 1. We hereafter refer to these three molecular species (HC_5N, CCS, HC_7N) as carbon chains throughout the rest of this paper.

Transition	Rest Frequency (GHz)	Channel Width (Km/s)
HC_5N $J = 9 \rightarrow 8$	23.96	0.40
CCS $J_N = 2_1 \rightarrow 1_0$	22.34	0.42
HC_7N $J = 20 \rightarrow 19$	22.56	0.42
HC_7N $J = 21 \rightarrow 20$	23.86	0.16

Table 1. Properties of the carbon chain transitions we observed towards our 12 sources.

2.2. *Target Properties*

The 12 molecular cloud clumps that we observed all have masses greater than 400 $M_\odot$ (Svoboda et al. 2019). The mass required for a clump to form a high-mass star is about 320 $M_\odot$ (Svoboda et al. 2016), so we do not deem these 12 clumps to be incapable of HMSF based on an insufficient mass. These clumps all have kinetic temperatures in a range of 10-17 K and

average densities that range from $n(H_2) = 1 \times 10^3$ cm^{-3} to $n(H_2) = 1 \times 10^4$ cm^{-3} (Svoboda et al. 2019). All of these 12 sources except G28539, were subsequently discovered to have CO outflows, which is an indicator of protostellar activity and the protostars within these clumps have been determined to be low-mass protostars (Svoboda et al. 2019). Thus, these clumps are no longer classified as Starless Clump Candidates, but we refer to them, rather, as 70 μm dark clumps (SMDC).

The source G23605 could have been misidentified as a SMDC in the Bolocam Galactic Plane Survey and it is possible that it is an evolved AGB star or an extra-galactic source of some sort and not actually a high-mass molecular cloud clump. For this reason, we exclude G23605 from our analysis and discussion in the following sections and only consider the other 11 sources. The carbon chain spectra of G23605, however, are shown for completeness.

3. METHODS

We extract the carbon chain spectra from our VLA data using two methods: (1) masking and (2) velocity registration. The spectra for carbon chains are faint, being about 3 times brighter than the single-beam RMS, and spread out over a large area, with the scale of these clumps being around 1 pc. This can be seen in the moment 0 map of CCS for the source G28539, which is shown in Figure 2. This moment 0 map of CCS shows the faint, extended signal from CCS in this source, and the other 10 sources have similarly faint and extended carbon chain emission. Because the signal from the carbon chains in these sources has low signal to noise per pixel and are spread out over a wide field, averaging techniques are required to be able to detect the carbon chain spectral lines. More specifically, the masking averaging method is necessary to spatially register the signal and improve the signal to noise ratio of the carbon chain spectra.

The first averaging technique we use to extract the carbon chain spectra from the VLA data is masking. The carbon chain data cubes were masked based on the moment 0 map of NH_3 such that only pixels above a 3σ brightness threshold, which corresponds to a value of approximately .015 Jy bm^{-1} Km s^{-1}, on the NH_3 moment 0 map were summed into the carbon chain spectra. We use NH_3 as a template for the mask because the NH_3 emission is much brighter than the carbon chains, $\approx$ 5 times brighter in these sources, and from comparing moment 0 maps, the carbon chains seem to follow the same spatial distribution as NH_3 in these clumps. Once the pixels below the brightness threshold were masked, the flux from pixels within the 3σ brightness threshold were summed along the spatial axis.

The brightness threshold can be seen as the yellow contour line on the moment 0 map of NH_3 of source G23297 in Figure 1. This yellow contour line shows which pixels were masked and which were summed into the spectra for this source. This masking method was used for all of the SMDC sources. The flux from each pixel within the yellow contour line are summed into the carbon chain spectra, while the flux from pixels outside of the yellow contour line in Figure 1 were not summed into the carbon chain spectra. This averaging technique increases the signal to noise ratio of the carbon chain spectra.

The second method that was used to obtain the carbon chain spectra was velocity registration. Since these molecular clumps are turbulent and have velocity fields, emission from the carbon chains occur at different velocities, which mixes signal and noise. The velocity registration method accounts for the velocity field of the clumps and improves the signal to noise ratio of the carbon chain spectra.

To account for the turbulence of the clumps, we register the flux from the carbon chains to the mean velocity of the moment 1 map of NH_3 of each of the clumps. This is done by calculating the velocity difference between each pixel, that is within the 3σ mask, of the NH_3 moment 1 maps and the mean velocity of the moment 1 maps and then shifting the spectra of each pixel by that velocity difference. By shifting the spectra of each pixel, the signal is all registered to the mean velocity of the moment 1 maps of NH_3. Once the spectra of each pixel have been shifted to the mean velocity of the moment 1 maps, the spectra of each pixel are then re-grid to a common spectral axis using the "nearest" interpolation method. The spectra of each pixel are then summed together across the spatial axis.

The effects of the velocity registration method can be seen in Figure 3, which shows the spectra of HC_5N from G30660, with the left spectrum being from the masking method and the spectrum on the right being obtained using the velocity registration method. This shows that the velocity registration method does give better signal to noise ratio by accounting for the the velocity field in the clump. The velocity registration method most likely does not bias the total flux value of the carbon chain spectral lines, since it is moving flux to a common velocity based on the moment 1 map of the clumps, and is not adding or removing signal or noise from the spectra.

Both the masking method and velocity registration method were used on the spectra of all three carbon chain molecules: HC_5N, CCS, and HC_7N. For the analysis of the spectra, all were obtained with the masking method except the spectra for G22695, G30120, and G30660 were obtained using the velocity registration method since these three sources had faint lines with just the masking method and velocity registration was necessary to get a better signal to noise ratio.

The spectra were then all fit with Gaussians and the best fit Gaussians were integrated to determine the total integrated intensity of each of the spectral lines. Both the masking method and velocity registration method are consistent with each other in that all the carbon chain detections obtained with the velocity registration method were also detected using the masking method. The total integrated intensity of the spectra using the two methods were also consistent with each other, meaning they were within the uncertainties.

4. RESULTS

4.1. *Molecule Detections*

We detect HC_5N and CCS in 11 out of 12 of our molecular clump sources, with the only non-detection being G23605, which we leave out of our analysis and discussion for reasons

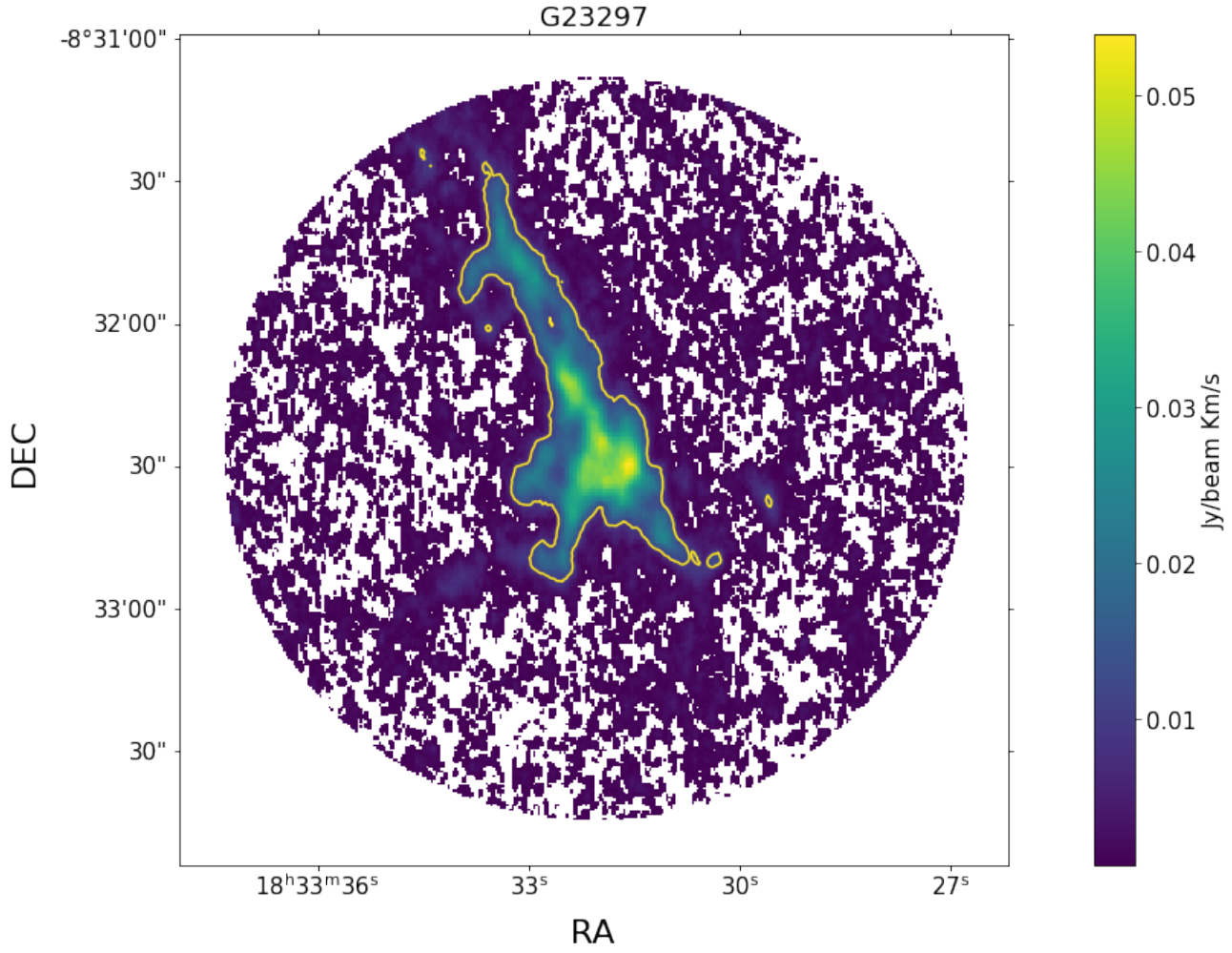

Figure 1. Moment 0 map of ammonia for G23297. Yellow contour line indicates the brightness threshold that was used for the masking technique. All pixels within the yellow contour line were summed into the carbon chain spectra, while all pixels outside of the yellow contour line were left out of the summation. This technique was used on all our sources.

previously mentioned. We consider a molecule to be detected if we observe a 5σ line across multiple channels. The brightness of the HC_5N and CCS spectra vary over all 11 of our sources, which can be seen in the spectra of HC_5N shown in Figure 4 and the spectra of CCS shown in Figure 5. The brightest HC_5N spectrum occurs in the source G30912 and the brightest CCS spectrum is in G28565, while the dimmest HC_5N spectrum occurs in G30120 and the dimmest CCS spectrum occurs in G30660.

All the HC_5N and CCS spectra that were detections were fit with Gaussians using the Gaussian fitting algorithm in PySpecKit (Ginsburg & Mirocha 2011) and from these fits, the total integrated intensity was computed using the equation for integrating a Gaussian. The results from the Gaussian fits and total integrated intensity calculations can be seen in Table 4.1. The total integrated intensities shown in this table are the integrated intensities that are used in the column density calculations.

While we detected HC_5N and CCS in all of our sources, we did not have clear detections of HC_7N in any of our sources, as all of our HC_7N lines were beneath the 5σ threshold for a detection. We further checked for HC_7N by averaging together the HC_7N spectra from all of our 11 sources. We average both HC_7N transitions we observed, $J = 20 \rightarrow 19$ and $J = 21 \rightarrow 20$, from all of our sources by velocity registering each spectra and re-gridding all the HC_7N spectra to a common spectral axis with the same spectral resolution and number of channels and then averaging all 22 HC_7N spectra together. The purpose of this averaging is to get a better signal to noise ratio in the HC_7N spectra and see if it yields a detection.

Averaging all the HC_7N spectra together does in fact show a detection, on average, in our sources. We have to be careful interpreting this result, since it is all the sources averaged together, but it does show that there is an HC_7N detection within these sources. The average spectra of HC_7N is shown in Figure 6. This figure also shows that the averaging of all the HC_7N spectra together, does in fact reduce the noise by about a factor of 5. We cannot tell which of our sources have HC_7N, due to the nature of averaging the spectra together, but this result does show that HC_7N is detected and present in some of these molecular clumps.

4.2. *Column Density Calculations*

Using the total integrated intensity of each line calculated by integrating the best fit Gaussian to the spcetra, we calculate the column densities of HC_5N and CCS. We calculate the column density of HC_5N assuming an optically thin line, using the equation for the column density of the upper level J_u of a linear molecule from (Walmsley et al. 1980):

$$N(J_u) = 8.348 \times 10^{16} \frac{(2J_u - 1)}{J_u^2} \frac{\int T_B dv}{\mu^2 B}, \qquad (1)$$

where J_u is the upper level in the transition $J_u \rightarrow J_{u-1}$, μ is the dipole moment in debye, $\int T_B dv$ is the integrated intensity of the spectra, and B is the rotational constant in MHz. We use B=1331.33 MHz and $\mu = 4.33$ D for the HC_5N $J = 9 \rightarrow 8$ transition, which are taken from Alexander et al. (1976). To calculate the total column density, we use the relation between the column density of a molecule in the upper energy state and the total column density of a molecule from Mangum & Shirley (2015) which is given as

$$\frac{N_{tot}}{N_u} = \frac{Q_{rot}}{g_u} e^{\frac{E_u}{kT_{ex}}} \qquad (2)$$

where g_u is the degeneracy of the energy state, which is $2J+1$, k is the Boltzmann constant, E_u is the energy of the upper state, T_{ex} is the excitation temperature, and Q_{rot} is the rotational partition function of a linear molecule which is given as

$$Q_{rot} = \frac{kT}{hB} e^{\frac{hB}{3kT}} \qquad (3)$$

where T is the excitation temperature and h is Planck's constant. We use $E_u = 5.75K$ for the HC_5N $J = 9 \rightarrow 8$ transition and $E_u = 1.606K$ for the CCS $J_N = 2_1 \rightarrow 1_0$ transition, which are taken from Alexander et al. (1976) and Saito et al. (1987).

We cannot assume local thermodynamic equilibrium (LTE) since these clumps have average densities of 1×10^3 - 1×10^4 cm^{-3}, which are lower than the carbon chains transitions' critical densities and collisions between molecules would be too infrequent for LTE to be achieved. By using RADEX (van der Tak et al. 2007), which is a one-dimensional non-LTE radiative transfer code for performing statistical equilibrium calculations, we determine that HC_3N is subthermally populated in conditions similar to those of these clumps, so we would expect HC_5N and CCS to be subthermally populated as well. Since these sources are not dense enough to assume LTE, we use the excitation temperature of NH_3 instead of the gas kinetic temperature of the clumps in the column density calculations.

We use a range of excitation temperatures of 4-6 K, which is used to determine the uncertainties in the column densities since we are not certain about the value of the excitation temperature of these clumps, but we expect that it is around 4 K. The column densities of CCS were calculated using the same rotational partition function and relation of upper energy column density to total column density, but the equation for the upper state column density (N_u) that was used for CCS is given as

$$\frac{N_u}{g_u} = \frac{3k \int T_B dv}{8\pi^3 \nu \mu^2 S} \qquad (4)$$

where ν is the frequency of the transition and S is the intrinsic line strength (Law et al. 2018). We use an intrinsic line strength of 1.98 for the CCS $J_N = 2_1 \rightarrow 1_0$ transition which is taken from Suzuki et al. (1992). For the rotational constant of CCS we use 6477.75 MHz and for the dipole moment we use 2.88 D, both of which were taken from Saito et al. (1987).

We also calculate the abundances to H_2 of these molecules using the calculated column densities. We calculate the abundances by converting our column densities into a molecular

Source	Molecule	T_B (K)	V_{LSR} (Km/s)	σ (km/s)	$\int T_B dv$ (K km/s)
G22695	HC_5N	0.114 (0.027)	77.59 (0.12)	0.44 (0.12)	0.13 (0.047)
G23297	HC_5N	0.182 (0.018)	55.18 (0.07)	0.67 (0.07)	0.31 (0.045)
G23481	HC_5N	0.073 (0.013)	63.98 (0.16)	0.76 (0.16)	0.14(0.039)
G24051	HC_5N	0.242 (0.018)	80.978 (0.056)	0.634 (0.056)	0.385 (0.044)
G28539	HC_5N	.0831 (0.0096)	88.451 (0.091)	0.681(0.091)	0.142 (0.025)
G28565	HC_5N	0.258 (0.026)	86.99 (0.095)	0.829 (0.095)	0.526 (0.082)
G29558	HC_5N	0.202 (0.019)	79.92 (0.057)	0.629 (0.057)	0.318 (0.029)
G29601	HC_5N	0.025 (0.007)	75.48 (0.43)	1.46 (0.43)	0.092(0.036)
G30120	HC_5N	0.05 0.012)	66.1 (0.2)	0.7 (0.2)	0.088 (0.033)
G30660	HC_5N	0.103 (0.008)	80.96 (0.048)	0.567 (0.048)	0.146 (0.016)
G30912	HC_5N	0.439 (0.046)	50.52 (0.07)	0.481 (0.046)	0.529 (0.067)
G22695	CCS	0.081 (0.025)	77.99 (0.36)	1.00 (0.36)	0.203 (0.096)
G23297	CCS	0.323 (0.021)	54.8 (0.05)	0.68 (0.05)	0.55 (0.054)
G23481	CCS	0.149 (0.014)	63.797 (0.08)	0.803 (0.088)	0.299 (0.043)
G24051	CCS	0.234 (0.024)	80.89 (0.067)	0.558 (0.067)	0.327 (0.052)
G28539	CCS	0.23 (0.019)	88.29 (0.058)	0.661 (0.058)	0.352 (0.044)
G28565	CCS	0.53 (0.03)	87.00 (0.049)	0.74 (0.049)	0.98 (0.085)
G29558	CCS	0.22 (0.019)	79.92 (0.094)	0.963 (0.094)	0.531 (0.052)
G29601	CCS	0.135 (0.009)	75.24 (0.058)	0.748 (0.058)	0.253 (0.026)
G30120	CCS	0.163 (0.016)	65.20 (0.099)	0.891 (0.099)	0.364 (0.054)
G30660	CCS	0.164 (0.011)	80.71 0(.046)	0.58 (0.046)	0.24 (0.025)
G30912	CCS	0.553 (0.057)	50.51 (0.041)	0.360 (0.044)	0.499 (0.079)

Table 2. Best fit parameters from Gaussian fits to carbon chain spectra. Uncertainties are shown in parenthesis.

mass for the entire clump and then dividing the total molecular mass of the carbon chains by the H_2 mass of the clumps which are taken from Svoboda et al. (2019). Uncertainty in the abundances are calculated by propagating the error of distance to the clump, clump mass, and column density using the general error propagation formula. The results of the column density and abundance calculations can be seen in Table 4.3.

We also look for trends in the column densities and abundances of each of the clumps and we compare them with the clump mass and temperature. The trends between HC_5N column density and temperature and CCS abundance and HC_5N can be seen in Figure 7. There appears to be a negative relationship between HC_5N column density and temperature and a positive relationship between CCS abundance and HC_5N abundance. We are not sure what causes the negative trend between HC_5N column density and temperature shown in the left plot in Figure 7. It does appear that sources that have a higher abundance of CCS tend to have a higher abundance of HC_5N as well, which is shown in the right plot in Figure 7.

4.3. *Comparison with Chemical Models*

We compare our calculated abundances of HC_5N and CCS to the UMIST 13 Dark Cloud Chemistry Models, which describe the abundance of molecules over the age of a dark molecular cloud (McElroy et al. 2013). Although grain surface chemistry does play a large role in the formation of various molecules, the UMIST 13 models do not include grain surface chemistry and only includes gas phase reactions because the many uncertainties involved prevent quantitatively accurate surface grain chemistry models (McElroy et al. 2013).

In comparing our measured abundances to the models, we find that our measured abundances for CCS are not in agreement with the chemical models and the abundance values disagree by about three orders of magnitude. It is noted by the authors of the UMIST 13 model that their model does not agree with previous measurements of CCS in dark clouds, so this is a well known issue (McElroy et al. 2013). The cause of the disagreement between the chemistry model and observations of CCS abundances is not clear, but it could be because sulfur is assumed to be more depleted than it actually is, the model is missing some key gas phase reactions that form CCS, or we speculate that the omission of dust grain chemistry in the model could cause the disagreement if there are grain surface reactions that are fundamental in the formation of CCS.

The measured abundance values of HC_5N from our sources, however, are comparable to the UMIST dark cloud chemistry model. We run two chemical models, both of which have all the same input parameters except the clump density. The input parameters that we use for the model are T=10 K, A_v=10, cos-

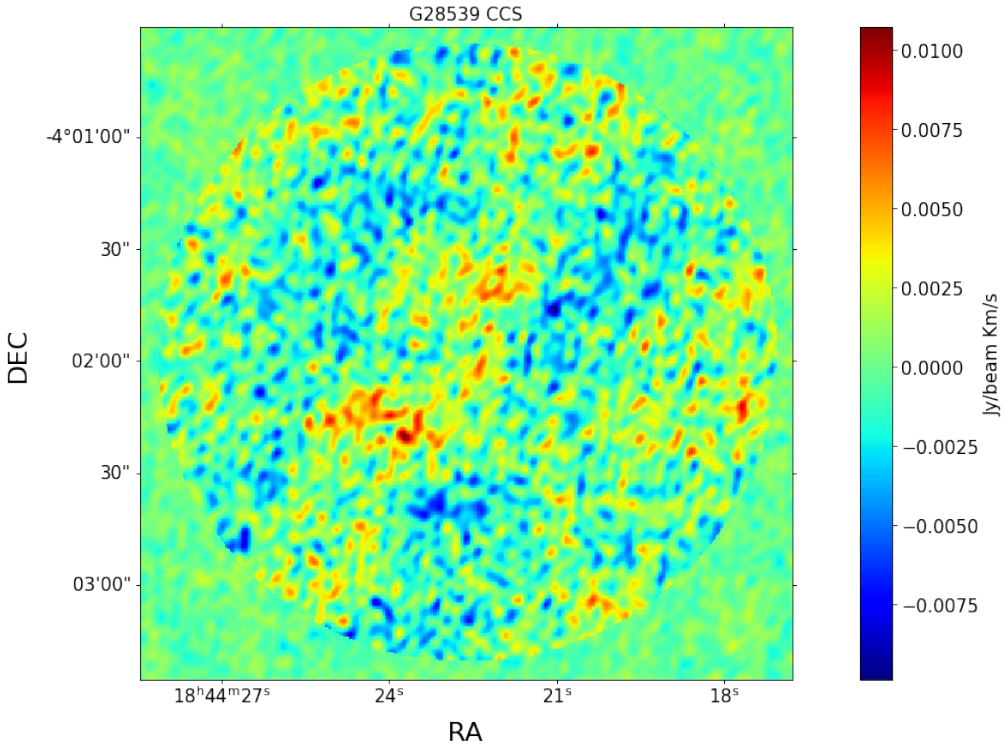

Figure 2. Moment 0 map of CCS for the source G28539. This map shows the faint spread out signal from CCS and thus the carbon chains have low signal to noise over a wide field of view. This is justification for why we employ the masking method to spatially register the carbon chain signal and get a better signal to noise ratio in the carbon chain spectra.

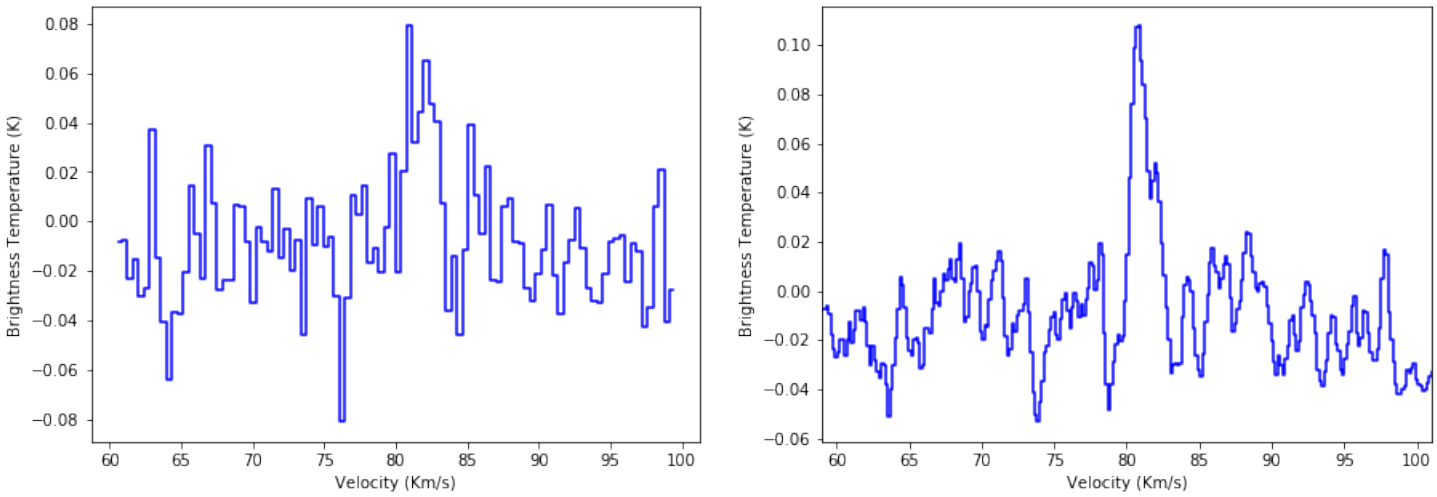

Figure 3. Plot of HC_5N spectra for G30660 with the spectrum on the left being obtained from the masking method and the spectrum on the right being extracted from the velocity registration method. This example shows how velocity registration gives better S/N by accounting for the velocity field of the clump.

mic ionization rate = standard galactic disk, UV radiation field = standard galactic disk, and initial abundances = atomic. We use two different cloud densities, one with n(H_2)=10^4 cm^{-3} and one with n(H_2)=10^3 cm^{-3}. We use multiply input densities because our sources have a range of densities between 10^3 cm^{-3} and 10^5 cm^{-3} with the higher density representing the density of the cores and the lower density representing the inter-core gas. We use n(H_2)=10^4 cm^{-3} as the density most representative of our 11 clumps.

The results of comparing our measured HC_5N abundances from the 11 sources with detections and the dark cloud chemistry models can be seen in Figure 8. Comparing with the n(H_2)=10^4 cm^{-3} favors that all of our 11 clumps with HC_5N detections are less than approximately 1 Myr old. The n(H_2)=10^3 cm^{-3} model favors that these 11 clumps are around 1 Myr, but the n(H_2)=10^4 cm^{-3} model is more representative of our clumps so it is most likely that our clumps are less than 1 Myr. We determine these maximum age limits by finding the age at which our measured abundances intersect the dark cloud chemistry models. The n(H_2)=10^3 cm^{-3} model does give an idea of the uncertainties involved in the dark cloud chemistry models and the uncertainty involved in our determination of the ages of these 11 clumps. These results from comparisons with the dark cloud chemical models suggest that these clumps have not yet had enough time to form high mass stars.

5. DISCUSSION

The detection of carbon chain molecules in all of our SMDC sources allows us to get an estimate of the evolutionary stage of these molecular clumps and answer the question regarding the age and HMSF efficiency of these SMDC sources. We use our HC_5N measured abundances to determine ages for the clumps and we do not use our measured CCS abundances for the age determination since our measured abundances do not agree with the UMIST 13 dark cloud chemistry model's predicted CCS abundances. The models do show that CCS does get depleted at similar timescales as HC_5N, after about 1 Myr, so our detection of CCS in all of our sources could be an indicator that the clumps are young (<1Myr) since CCS is also an early time carbon chain molecule (Sakai & Yamamoto 2013). Although our measured CCS abundances were three orders of magnitude greater than predicted by the dark cloud chemistry model, the detection of CCS in these sources could be in itself an indicator that these clumps are at early evolutionary stages in their lifetime.

By comparing our measured HC_5N abundances for our 11 sources with carbon chain detections and dark cloud chemistry models we determine that the 11 sources are most likely less than about 1 Myr old and are most likely between 10^4 and 1.5×10^6 years old. Comparing our HC_5N abundances to the models suggests that these 11 clumps with HC_5N detections are not old enough to be depleted in carbon chains, which the models show the abundance of HC_5N drops off below 1×10^{-10} at around 1×10^5 years for the n(H_2)=1×10^4 cm^{-3} density model and 1.5×10^6 years for the n(H_2)=1×10^3 cm^{-3} density model. Thus, we can conclude that with our measured abundances of HC_5N in these sources and the timescales of carbon chain depletion suggested by the dark cloud chemistry models, that these 11 SMDC sources are most likely $\lesssim 1$ Myr old.

A limitation to this method of determining ages of the molecular clumps are the uncertainties involved in the dark cloud chemistry models. Uncertainties in the abundances of dark cloud chemistry models are in the range of 1 order of magnitude for simple species, but can become larger for molecules with more atoms (Vasyunin et al. 2004). The uncertainties in the chemical models can also be seen in Figure 8 by comparing the lower density model to the higher density model. The change in input density by a factor of 10 does have an effect on the age that we determine for these clumps. Our sources have densities in a range that includes the densities of both models shown in 8, so the uncertainty in the models is relevant for the age determination of the clumps and is a limiting factor to this method of determine the evolutionary stage of these clumps.

To answer the question of whether or not these clumps are inefficient at forming high-mass stars, we use a statistical reasoning that it is unlikely that all of the clumps would inefficient at HMSF given that we measured them all to be young ($\lesssim$ 1Myr old). Since, if all of these clumps were inefficient at forming high-mass stars, they could have been any age and we would have expected their ages to be equally distributed over a wide age range (0-30 Myr). There is no reason why all the clumps would be young if they are inefficient at forming high-mass stars, thus, we think it is unlikely that all these clumps would be inefficient at high-mass star formation given that all 11 of them are less than approximately 1 Myr. This result favors that these clumps have not yet had time to form high-mass stars, and will potentially go on to form high-mass stars in their lifetime.

Ten out of the eleven clumps with carbon chain detections were previously observed to have CO outflows, which is a sign of low-mass protostellar activity within the clumps (Svoboda et al. 2019). This is important to note given that our observation of carbon chains in these clumps suggests that the clumps are less than approximately 1 Myr old. The result that these clumps are less than 1 Myr old and have low mass protostars within them, favors the idea that these clumps have had enough time to form low-mass stars but not yet enough time to form high-mass stars, since we deem that these clumps are all massive enough to form high-mass stars with masses greater than 400 $M_\odot$.

This finding is consistent with the idea that molecular cloud clumps go through a low-mass star formation phase early within the clump's lifetime ($\lesssim$ 1 Myr) and form low-mass stars first before high-mass stars. This result is also consistent with the idea that the clumps might actually never be starless and could form low-mass protostars while the clump itself is forming. If the process of clump formation is dynamic, then it is possible that low-mass stars form within the clump while the clump itself is forming and thus these clumps are never truly starless as they would have low-mass stars since their formation. Since our observations of carbon chains in

Source	Molecule	Column Density (cm^{-2} $*10^{12}$)	Abundance to H_2 ($*10^{-10}$)
G22695	HC_5N	1.42 (0.51)	2.49 (0.97)
G23297	HC_5N	3.38 (0.49)	17.4 (5.2)
G23481	HC_5N	1.53 (0.42)	9.02 (3.1)
G24051	HC_5N	4.20 (0.48)	14.8 (3.1)
G28539	HC_5N	1.55 (0.27)	3.12 (.69)
G28565	HC_5N	5.74 (0.89)	10.3 (3.1)
G29558	HC_5N	3.47 (0.32)	25.3 (5.2)
G29601	HC_5N	1.00 (0.39)	11.4 (5.2)
G30120	HC_5N	.959 (0.36)	3.78 (1.7)
G30660	HC_5N	1.59 (0.17)	3.72 (1.1)
G30912	HC_5N	5.77 (0.73)	13.2 (3.8)
G22695	CCS	1.78 (0.84)	2.34 (1.2)
G23297	CCS	4.82 (0.47)	18.6 (5.1)
G23481	CCS	2.62 (0.38)	11.6 (2.8)
G24051	CCS	2.86 (0.46)	7.57 (1.8)
G28539	CCS	3.08 (0.39)	4.64 (.87)
G28565	CCS	8.58 (0.74)	11.5 (3.1)
G29558	CCS	4.65 (0.46)	25.5 (5.3)
G29601	CCS	2.22 (0.23)	19.0 (4.9)
G30120	CCS	3.19 (0.47)	9.42 (2.7)
G30660	CCS	2.10 (0.22)	3.69 (1.1)
G30912	CCS	4.37 (0.69)	7.48 (2.3)

Table 3. Values for column density and abundance of HC_5N and CCS for each source with a detection. Uncertainties are reported in parenthesis.

these clumps favor that these clumps are less than approximately 1 Myr old and they are most likely not inefficient at forming high-mass stars and have been observed to have low-mass protostellar activity, we can say that these results are consistent with the idea that high-mass clumps go through a low-mass star formation phase with a timescale on the order of 1 Myr and then form high-mass stars after forming low-mass protostars.

6. CONCLUSION

We present the observation of molecular spectral lines of carbon chains towards 12 70 μm dark clumps that were previously identified via the Bolocam Galactic Plane Survey. We look for HC_5N, CCS and HC_7N in each of out 12 sources. The observation of carbon chains in these molecular cloud clumps is to probe the age of these clumps, since carbon chains are thought to be an early time species. Our main findings from these observations are:

1. We detect HC_5N and CCS towards 11 out of 12 of these molecular cloud clump sources, and the one source with a non-detection could possibly not be a molecular cloud clump and could rather be an AGB star or an extragalactic source.

2. We do not have any clear 5σ HC_7N detections, but averaging all the spectra from both transitions from all 11 sources with carbon chain detections shows that there is an HC_7N detection on average in these sources.

3. From comparing our measured abundances of HC_5N to dark cloud chemistry models, we find that these 11 sources are most likely less than 1 Myr old.

4. Since these 11 clumps were found to be young, we determine that it is unlikely that they all would be inefficient at forming high-mass stars and young, since if they were inefficient they could have been any age and evenly distributed across a range of ages.

5. The results that the clumps are less than 1 Myr and previous observations that found low-mass protostellar activity in these clumps are consistent with the idea that clumps go through low-mass star formation on timescales of less than 1 Myr and then form high-mass stars after forming low mass stars.

I would like to thank NRAO and the NSF for putting on the summer REU program. I would also like to thank my mentors Brian Svoboda, David Meier, and Juergen Ott for helping me throughout this project.

Facilities: VLA

Software: This research has made use of the following software projects: Astropy (The Astropy Collaboration et al. 2018), Matplotlib (Hunter 2007), NumPy and SciPy (Oliphant 2007), Pandas (McKinney 2010), IPython (Pérez & Granger 2007), CASA (McMullin et al. 2007), and the NASA's Astrophysics Data System.

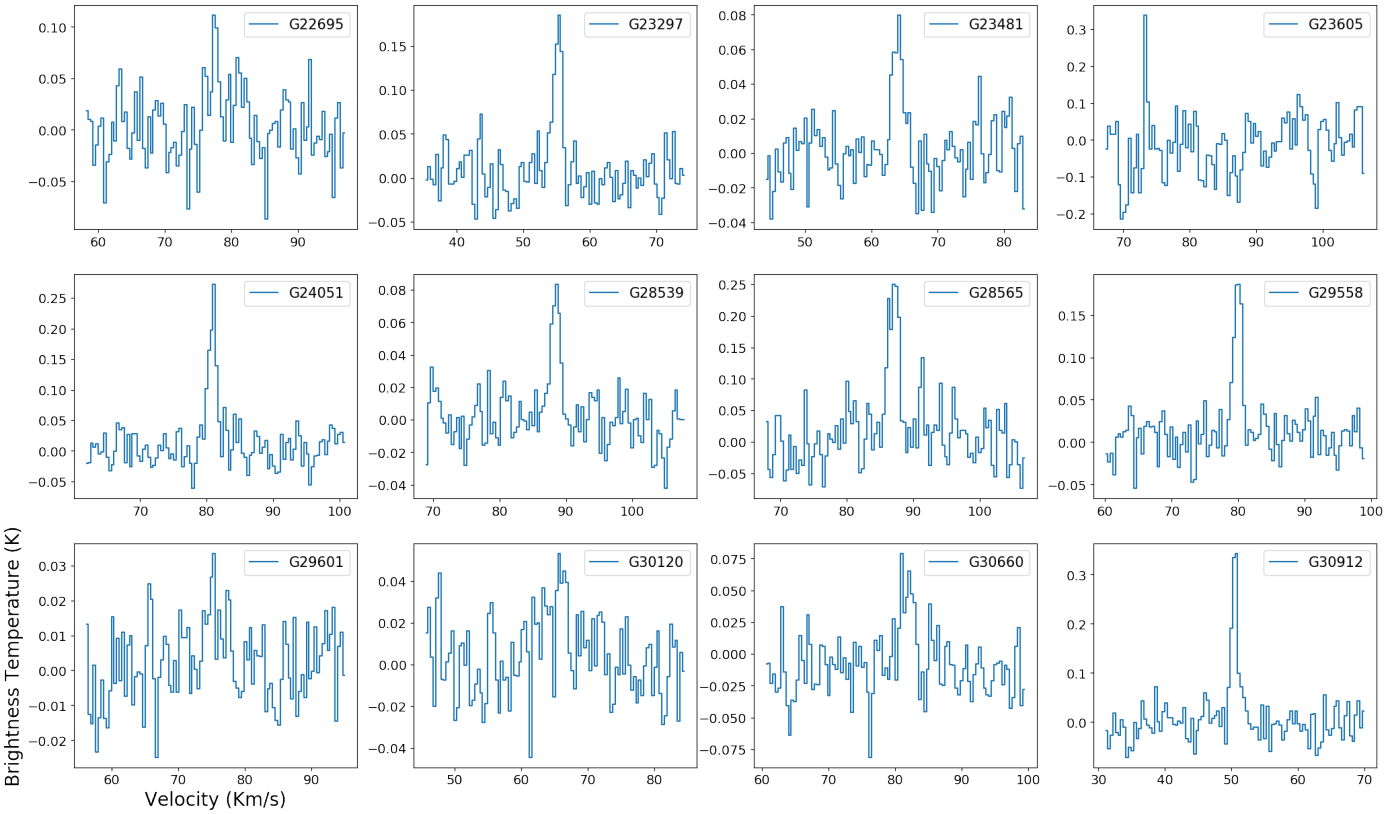

Figure 4. Spectra of HC_5N for all 12 of our sources. These spectra were obtained with the masking method. The only non-detection of HC_5N in on 12 sources occurs in G23605, which is the upper right hand corner spectrum in this figure. This source might not actually be a molecular cloud clump and could actually be an evolved star or extra-galactic source. The velocities on the x-axis of these spectra are radio local standard of rest velocities.

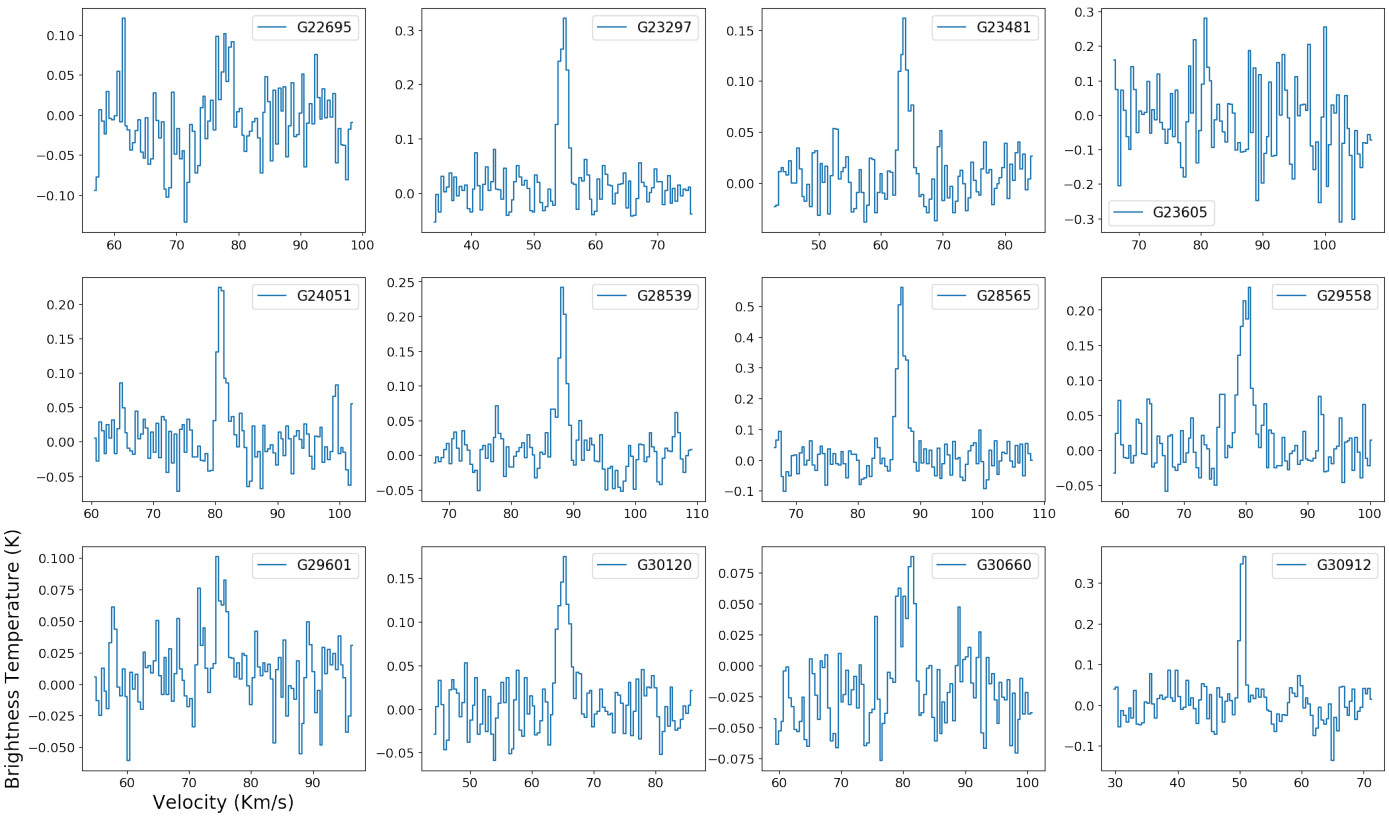

Figure 5. Spectra of CCS for all 12 of our sources. These spectra were obtained with the masking method. The only non-detection of CCS in on 12 sources occurs in G23605, which is the upper right hand corner spectrum in this figure. The velocities on the x-axis of these spectra are radio local standard of rest velocities.

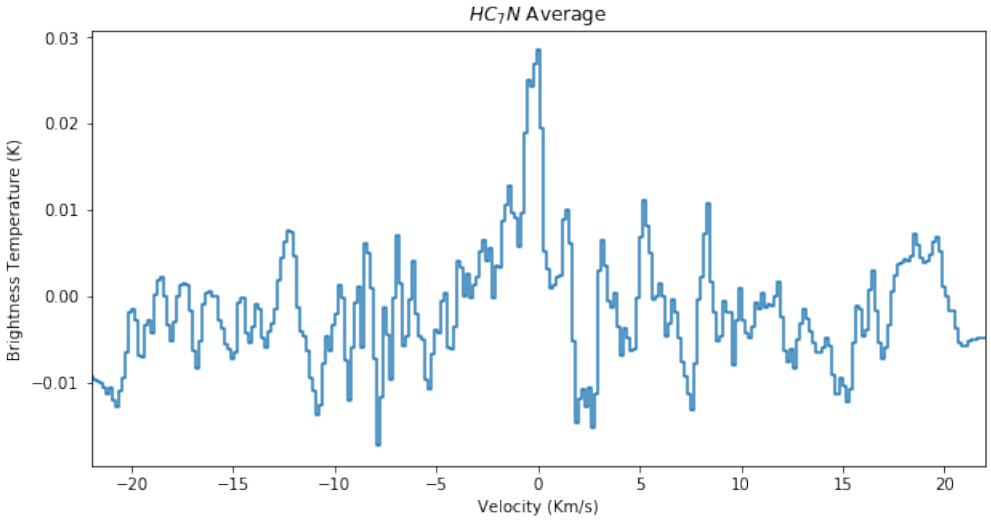

Figure 6. Averaged spectrum of HC_7N obtained by averaging both transitions, $J = 20 \rightarrow 19$ and $J = 21 \rightarrow 20$, of HC_7N for all sources that had an HC_5N detection.

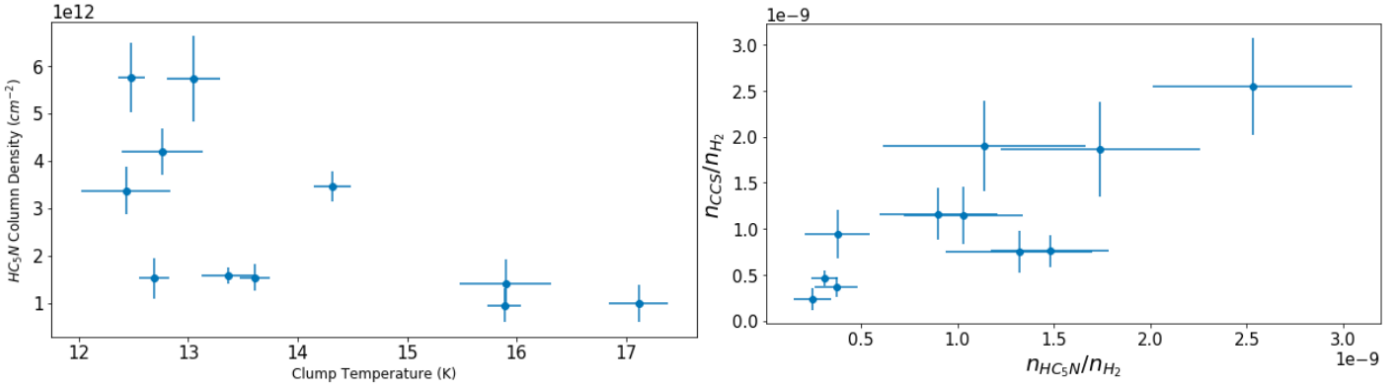

Figure 7. Plot on left shows HC_5N column density vs the clump kinetic temperature. There appears to be a downward trend between HC_5N column density and clump temperature. Figure on the right shows CCS abundance as a function of HC_5N abundance and there appears to be a positive trend between the two.

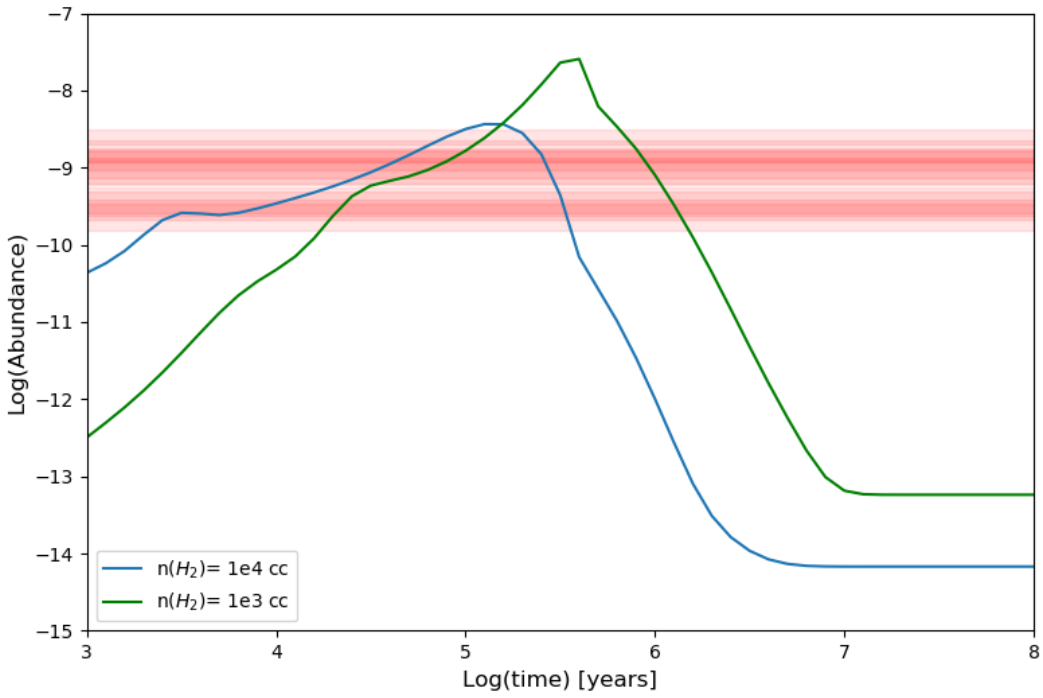

Figure 8. Plot of abundance of HC_5N as a function of age of the clump. The blue line shows the abundance over time predicted by the UMIST 12 chemistry model using a clump density of n(H_2)=10^4 cm^{-3} and the green line indicates a model with a density of n(H_2)=10^3 cm^{-3}. The red colored areas represent the measured abundances of each of our 11 sources with HC_5N detections and the colored area indicates the uncertainties in the abundances. The higher density model is more representative of our sources and comparing our measured abundances to this model suggests that these 11 clumps with carbon chain detections are less than 1 Myr old.

REFERENCES

Aguirre, J. E., Ginsburg, A. G., Dunham, M. K., et al. 2011, ApJS, 192, 4, doi: 10.1088/0067-0049/192/1/4

Alexander, A. J., Kroto, H. W., & Walton, D. R. M. 1976, Journal of Molecular Spectroscopy, 62, 175, doi: 10.1016/0022-2852(76)90347-7

Battersby, C., Bally, J., Jackson, J. M., et al. 2010, ApJ, 721, 222, doi: 10.1088/0004-637X/721/1/222

Bergin, E. A., & Tafalla, M. 2007, ARA&A, 45, 339, doi: 10.1146/annurev.astro.45.071206.100404

Beuther, H., Churchwell, E. B., McKee, C. F., & Tan, J. C. 2007, in Protostars and Planets V, ed. B. Reipurth, D. Jewitt, & K. Keil, 165. https://arxiv.org/abs/astro-ph/0602012

Ginsburg, A., & Mirocha, J. 2011, PySpecKit: Python Spectroscopic Toolkit. https://ascl.net/1109.001

Ginsburg, A., Glenn, J., Rosolowsky, E., et al. 2013, ApJS, 208, 14, doi: 10.1088/0067-0049/208/2/14

Hirota, T., Ohishi, M., & Yamamoto, S. 2009, ApJ, 699, 585, doi: 10.1088/0004-637X/699/1/585

Hunter, J. D. 2007, Computing In Science & Engineering, 9, 90, doi: 10.1109/MCSE.2007.55

Lada, C. J., & Lada, E. A. 2003, ARA&A, 41, 57, doi: 10.1146/annurev.astro.41.011802.094844

Law, C. J., Öberg, K. I., Bergner, J. B., & Graninger, D. 2018, ApJ, 863, 88, doi: 10.3847/1538-4357/aacf9d

Mangum, J. G., & Shirley, Y. L. 2015, PASP, 127, 266, doi: 10.1086/680323

McElroy, D., Walsh, C., Markwick, A. J., et al. 2013, A&A, 550, A36, doi: 10.1051/0004-6361/201220465

McKinney, W. 2010, in Proceedings of the 9th Python in Science Conference, ed. S. van der Walt & J. Millman, 51 – 56

McMullin, J. P., Waters, B., Schiebel, D., Young, W., & Golap, K. 2007, in Astronomical Society of the Pacific Conference Series, Vol. 376, Astronomical Data Analysis Software and Systems XVI, ed. R. A. Shaw, F. Hill, & D. J. Bell, 127

Motte, F., Bontemps, S., & Louvet, F. 2018, ARA&A, 56, 41, doi: 10.1146/annurev-astro-091916-055235

Oliphant, T. E. 2007, Computing in Science & Engineering, 9

Peretto, N., & Fuller, G. A. 2009, VizieR Online Data Catalog, J/A+A/505/405

Pérez, F., & Granger, B. E. 2007, Computing in Science & Engineering, 9

Rosolowsky, E., Dunham, M. K., Ginsburg, A., et al. 2010, ApJS, 188, 123, doi: 10.1088/0067-0049/188/1/123

Saito, S., Kawaguchi, K., Yamamoto, S., et al. 1987, ApJL, 317, L115, doi: 10.1086/184923

Sakai, N., & Yamamoto, S. 2013, Chemical Reviews, 113, 8981, doi: 10.1021/cr4001308

Smith, R. J., Longmore, S., & Bonnell, I. 2009, MNRAS, 400, 1775, doi: 10.1111/j.1365-2966.2009.15621.x

Suzuki, H., Yamamoto, S., Ohishi, M., et al. 1992, ApJ, 392, 551, doi: 10.1086/171456

Svoboda, B. E., Shirley, Y. L., Battersby, C., et al. 2016, ApJ, 822, 59, doi: 10.3847/0004-637X/822/2/59

Svoboda, B. E., Shirley, Y. L., Traficante, A., et al. 2019, ApJ, 886, 36, doi: 10.3847/1538-4357/ab40ca

Taniguchi, K., Herbst, E., Caselli, P., et al. 2019, ApJ, 881, 57, doi: 10.3847/1538-4357/ab2d9e

Taniguchi, K., Saito, M., Sridharan, T. K., & Minamidani, T. 2018, ApJ, 854, 133, doi: 10.3847/1538-4357/aaa66f

The Astropy Collaboration, Price-Whelan, A. M., Sipőcz, B. M., et al. 2018, AJ, 156, 123, doi: 10.3847/1538-3881/aabc4f

van der Tak, F. F. S., Black, J. H., Schöier, F. L., Jansen, D. J., & van Dishoeck, E. F. 2007, A&A, 468, 627, doi: 10.1051/0004-6361:20066820

Vasyunin, A. I., Sobolev, A. M., Wiebe, D. S., & Semenov, D. A. 2004, Astronomy Letters, 30, 566, doi: 10.1134/1.1784498

Walmsley, C. M., Winnewisser, G., & Toelle, F. 1980, A&A, 81, 245